

# The development of volcanic ash cloud layers over hours to days due to turbulence layering

Marcus Bursik <sup>1,\*</sup>ORCID:0000-0002-9312-5202,

Qingyuan Yang<sup>2</sup> Adele Bear-Crozier <sup>3</sup>, Michael Pavolonis<sup>4</sup> and Andrew Tupper <sup>3</sup>

<sup>1</sup>Center for Geohazards Studies,

University at Buffalo, Buffalo NY USA

<sup>2</sup>Earth Observatory of Singapore,

Nanyang Technological University, Singapore

<sup>3</sup>Bureau of Meteorology, Melbourne, Australia

<sup>4</sup>NOAA Cooperative Institute for Meteorological Satellite Studies

University Wisconsin, Madison WI USA

January 1, 2021

## Abstract

Volcanic ash clouds often become multilayered and thin with distance from the vent. We explore one mechanism for development of this layered structure. We review data on the characteristics of turbulence layering in the free atmosphere, as well as examples of observations of layered clouds both near-vent and distally. We then explore dispersion models that explicitly use the observed layered structure of atmospheric turbulence. The results suggest that the alternation of turbulent and quiescent atmospheric layers provides one mechanism for development of multilayered ash clouds by modulating vertical particle motion. The largest particles, generally  $> 100\mu\text{m}$ , are little affected by

turbulence. For particles in which both settling and turbulent diffusion are important to vertical motion, mostly in the range of 10-100  $\mu\text{m}$ , the greater turbulence intensity and more rapid turbulent diffusion in some layers causes these particles to spend greater time in the more turbulent layers, leading to a layering of concentration. For smaller particles, mostly in the submicron range, the more rapid diffusion in the turbulent layers causes these particles to “wash out” quickly.

## 1 Introduction

Volcanic ash is a multi-billion dollar economic hazard to aviation, as shown during the 2010 eruptions of Eyjafjalla-jökull, Iceland [Casadevall, 1994; Mazzocchi *et al.*, 2010]. It is also a risk to flight safety, with hundreds of encounters of varying severity recorded, and several instances of multiple engine flame-out in flight. The International Airways Volcano Watch (IAVW), which seeks to safely separate aircraft from volcanic ash in flight, relies on detecting areas of ash and forecasting its future movement [Tupper *et al.*, 2007]. However, the forecasting of ash presence and concentration is generally poorly resolved vertically, although there is some progress in this direction, e.g., [Heinold *et al.*, 2012; Kristiansen *et al.*, 2015]. Aircraft flying in a supposedly ash-contaminated region at a particular altitude may encounter no ash or significant and potentially damaging amounts, due to the high degree of ash stratification with altitude. The improved understanding and forecasting of stratification would assist enormously in managing the hazard and support the continuing development of the IAVW.

Photography and satellite imagery of numerous volcanic eruptions show that a single or multiple layered structure is a fundamental aspect of volcanic cloud development [Carazzo and Jellinek, 2013]. Aerial as well as ground-based photography have been particularly useful near the volcano to elucidate this layering. Lidar backscatter data have been key in defining the layered structure in distal regions, particularly those from the CALIOP (Cloud-Aerosol Lidar with Orthogonal Polarization) instrument (Fig. 1, 2). Volcanic layers can be stratospheric as well as tropospheric [Winker and Osborn, 1992].

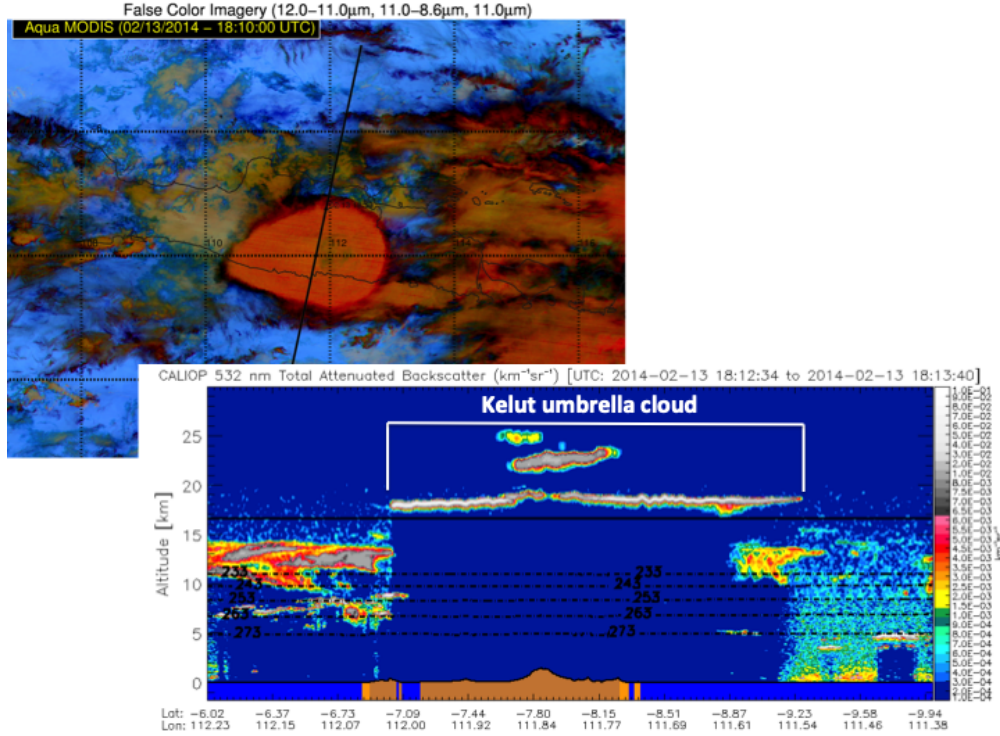


Figure 1: (a) Aqua-MODIS RGB false color image of Java capturing Kelud umbrella cloud on 13 February, 2014 (red hues). (b) CALIOP nadir LIDAR total attenuated backscatter (along track shown in (a) with solid line) showing isotherms (kelvin, black dotted lines) and tropopause (black solid line). Clouds between 10-15 km on South (right) side under umbrella cloud could be of volcanic origin.

Multiple layers are thought to form and separate by numerous processes, some unique to volcanic clouds. The primary volcanic cloud layer near the vent, such as the volcanic umbrella cloud or anvil cloud, arises from the driving of hot eruptive gas and ash parcels outward around their equilibrium level, or neutral buoyancy height [Sparks *et al.*, 1997]. As suggested by brightness temperatures over the surface of near-vent clouds and ground based photography, umbrella clouds can be solitary, accompanied by a single lower intrusion resulting from re-entrainment and column-edge downflow [Woods and Kienle, 1994; Bursik, 1998] or accompanied by lower level skirt clouds [Barr, 1982], which may or may not contain ash. Ash accretion, ash re-entrainment and source variability – injection of ash at different altitudes with changing eruption rate and wind fields, cause development of multiple layers [Holasek *et al.*, 1996a; Tupper

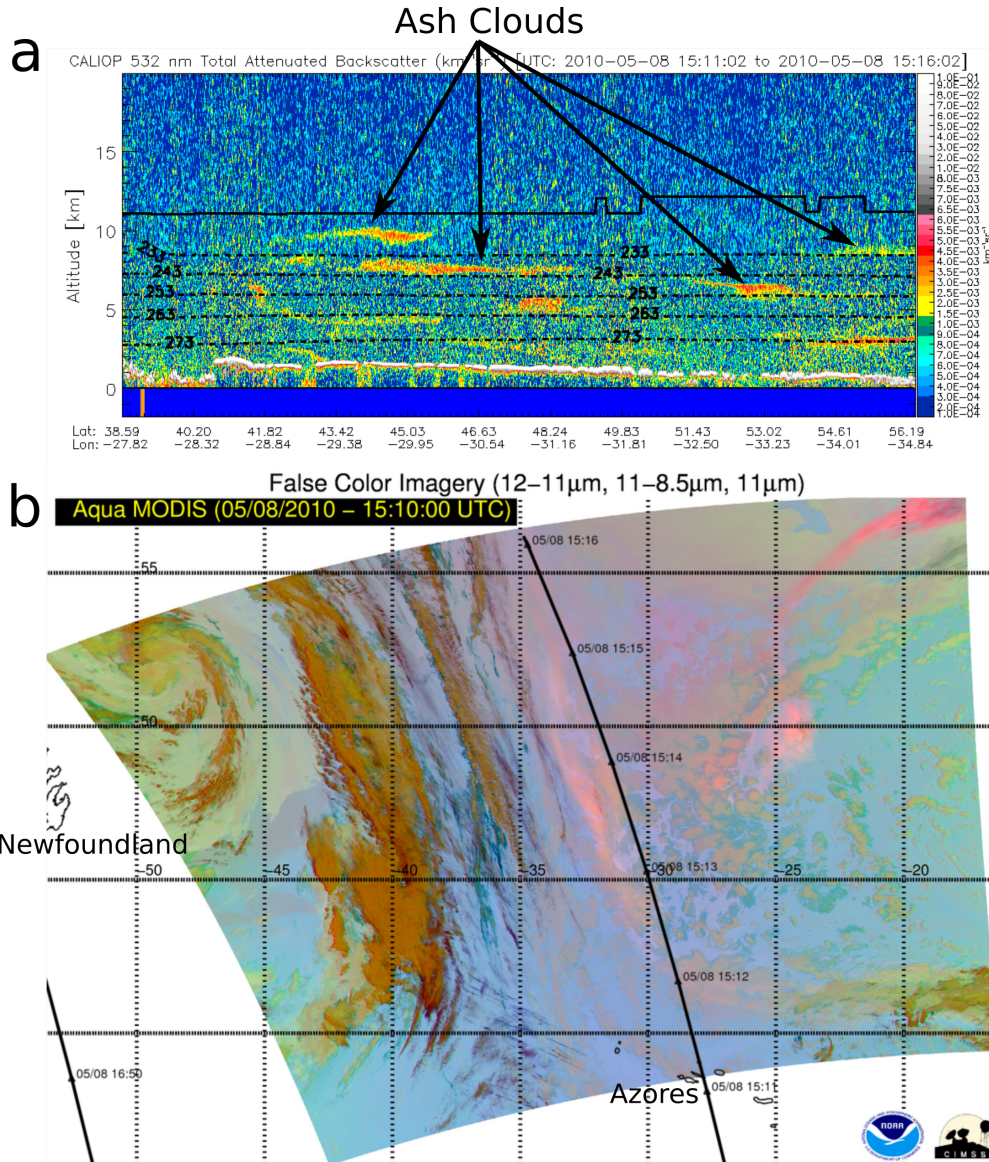


Figure 2: **(a)** CALIOP nadir LIDAR total attenuated backscatter (along track shown in **(b)**) showing complex layering of Eyjafjallajokull ash cloud on 8 May, 2010, isotherms (kelvins, black dotted lines) and tropopause (black solid line). **(b)** Aqua-MODIS RGB false color image [Pavolonis *et al.*, 2013] of North Atlantic capturing this ash cloud (pink hues).

*et al.*, 2004; Thorsteinsson *et al.*, 2012]. Mechanical unmixing of particulate-laden and gaseous volcanic cloud components, or gas-ash separation, has been noted as a further cause of volcanic layer formation [Holasek *et al.*, 1996b; Fero *et al.*, 2009], perhaps enhanced by gravity current slumping of the particle laden component [Prata *et al.*, 2017]. Double diffusion and convective sediment flux to a single [Woods and Kienle,



1994; Bursik, 1998; Hoyal *et al.*, 1999a, b; Carazzo and Jellinek, 2012] and multiple [Carazzo and Jellinek, 2013] levels by descending fingers that intrude below the level of a major volcanic cloud layer have been observed, and recreated in the laboratory.

Further from the vent,  $\sim > 500$  km and hours in transport time, downward looking satellite sensors are used for cloud tracking, but these penetrate only partially into the highest layer of an optically thick cloud, and satellite remote sensing algorithms are most sensitive to the column integrated ash properties, even when multiple optically thin layers are present. Although horizontal, planview resolution can thus be good, satellite data and often volcanic ash transport and dispersal models (VATDs), used to forecast future position, have difficulty in reproducing the vertical structure of distal volcanic clouds [Devenish *et al.*, 2012; Folch *et al.*, 2012; Heinold *et al.*, 2012]. Numerical inversion of VATDs has been used to map distal cloud positions seen in CALIOP and other data to time-varying release height from the source vent ([Stohl *et al.*, 2011; Kristiansen *et al.*, 2015; Zidikheri *et al.*, 2017, 2018]. Dacre *et al.* [2015] used a new scheme to calculate clear-air turbulence (CAT) in the numerical weather prediction (NWP) model used to drive the NAME VATD model. Numerous distal clouds from the Eyjafjallajökull eruption were analyzed and thought to be controlled in thickness by an interaction between wind shear, which acted to thin layers, and turbulent diffusion, acting to thicken them [Dacre *et al.*, 2015].

## 1.1 Problem Statement

A correct understanding of layer formation and morphology is critical for any attempt to construct VATD models capable of producing output consistent with observations of vertical ash distribution, yet the formation mechanisms of atmospheric ash cloud layers are not fully understood. One potential mechanism for their formation and characteristics is the subject of the present contribution. Our working hypothesis is that, because particle settling and atmospheric turbulence act to varying degrees in a layered atmosphere, the turbulence structure of the atmosphere can cause ash layer formation, through the process of enhanced suspension in vertically restricted regions of high turbulence.

## 2 Materials and Methods

### 2.1 Background Materials

#### 2.1.1 Atmosphere

Ash transport occurs in the large-scale structures of the wind field, while ash dispersion or spread is caused by the small-scale turbulence structures and eddies [Bursik, 1998; Harvey *et al.*, 2018]. The free atmosphere itself, with or without volcanic clouds, generates small-scale turbulent eddies. Eddies are generally created in the troposphere by Rayleigh-Taylor (convective) instabilities associated with clouds, and can be found 33% of the time [Vasseur and Vanhoenacker, 1998]. In the stratosphere, clear-air turbulence (CAT) is primarily thought to be generated by breaking of upward-propagated gravity waves from the troposphere or tropopause, i.e., the Kelvin-Helmholtz mechanism, acting during episodes of vertical wind shear in the horizontal wind components [Barat, 1982; Nastrom and Eaton, 1993; Sato *et al.*, 1995]. In volcanic clouds near the vent, turbulence is created by both the Rayleigh-Taylor and Kelvin-Helmholtz mechanisms, as ash clouds intrude into the atmosphere as gravity currents. Kelvin-Helmholtz instability is driven by the shear between the intruding cloud and the atmosphere [Britten and Simpson, 1981]. Rayleigh-Taylor instability is driven by cloud top convective instabilities [Vasseur and Vanhoenacker, 1998], convective sedimentation, fingering and local, eddy scale density reversal [Woods and Kienle, 1994; Holasek *et al.*, 1996b; Chakraborty *et al.*, 2006].

In the free atmosphere, parameters such as moisture content and temperature do not change monotonically with height; there are layers of relatively homogeneous air, separated by regions in which parameters vary rapidly [Vasseur and Vanhoenacker, 1998; Sharman *et al.*, 2012]. Both the stratosphere and the troposphere are layered in this way on scales of  $\mathcal{O}[0.1 - 1\text{km}]$  [Maekawa *et al.*, 1993; Wilson *et al.*, 2014], although the layers in the troposphere tend to be more transient and discontinuous [Gage *et al.*, 1980]. Information of sufficient resolution in the vertical direction to discern and characterize the turbulence layered structure is obtained from airborne

measurement campaigns or rawinsonde balloon releases [*Dehghan et al.*, 2014; *Cho et al.*, 2003; *Pavelin et al.*, 2002]. Several methods have been developed to derive turbulence from rawinsonde and other high-resolution data. *Vasseur and Vanhoenacker* [1998] measured changes in the refractive index structure parameter for radio waves, as turbulence causes changes in the refractive index, based on rawinsonde pressure, temperature, humidity, wind speed and wind direction data. *Clayson and Kantha* [2008] used variations in the potential temperature profile from an idealized profile to calculate the Thorpe scale, and derive turbulent dissipation and diffusivity. These estimates can be made for single rawinsonde profiles with simple calculations. In the troposphere, layers of constant relative humidity (RH) or mixing ratio,  $q$ , can act as tracers for high turbulence [*Cho et al.*, 2003]. This is because as turbulence intensifies, mixing intensifies, and tracers become more evenly distributed throughout a layer. The macroscopic mixing caused by turbulence acts as a diffusive process, which is characterized by a (turbulent) eddy diffusivity,  $\kappa$ . (Atmospheric moisture is also important in aiding plume lift, especially in plumes from weak sources, or at low latitude, where the moisture content is high [*Sparks et al.*, 1997; *Tupper et al.*, 2009]. High RH layers might therefore indicate not only turbulence, but also particularly intense reservoirs of energy available for plume lift.) As a result of the layering, large-volume or bulk turbulence, and the eddy diffusivity,  $\kappa$ , that expresses its intensity, is highly anisotropic ( $\kappa_h \gg \kappa_z$ ), and only within thin, well-defined layers is it approximately isotropic ( $\kappa_{h,local} \approx \kappa_{z,local}$ ) [*Gage et al.*, 1980].

There are drawbacks to extrapolating high-resolution or point data to a regional scale because of spatial and temporal inhomogeneity; the troposphere is highly transient and spatially variable [*Clayson and Kantha*, 2008; *Thouret et al.*, 2000]; tropospheric isobaric surfaces are not necessarily parallel to the earth's surface, especially at fronts and in mountain waves *Sharman et al.* [2012]. Fronts are associated with tropopause folds, non-horizontal isobaric surfaces separating cold from warm air, and turbulence in folds is generated by local dynamic and convective instabilities. Mountain waves form as the density stratified atmosphere flows past the lee side of a mountain or mountain range. These waves can break, resulting in local turbulence concentrated in

non-horizontal layers.

### 2.1.2 Ash Clouds

Data are available from a number of sources on the shape and structure of both near-vent and distal ash clouds. In the near-vent region, data tend to be more limited, due to the lower optical depth. Nevertheless, cloud brightness temperature (BT) as measured from nadir-looking geostationary and low-earth orbiting satellites provides useful information, as the topography of the top of the near-vent clouds can be quite variable, with a distinct high point or swell above the central vent that might be many kilometers above the top of the main umbrella cloud [Fero *et al.*, 2009]. In addition, airborne and ground-based photography and videography have provided extensive data on the features at the base of the main umbrella or anvil, and within the underlying cloud layers. Visible satellite imaging of the near vent cloud top consistently reveals strong, well-defined three-dimensional vortex structures above the vent, which evolve to smooth, somewhat more diffuse structures in the umbrella cloud [Pouget *et al.*, 2016].

Although the air can be choked with opaque, diffuse ash bodies that extend to ground level near vent, and although gravitational intrusions, such as umbrella clouds, are wedge-shaped by nature and therefore of variable depth, measurements have been made of the  $\Delta BT$  between cloud top and edge of the main cloud. The results suggest that umbrella clouds at the vent typically encompass depths of  $\mathcal{O}[5]$  km (Table 1), which makes a large mass of ash available for transport at multiple levels. Some of the lower near-vent clouds also become distal clouds. In some cases, it might be possible to find the entire troposphere and even lower stratosphere charged with ash, or only a distinct layer or two of  $\mathcal{O}[1 - 10]$  km depth.

In the distal region, airborne lidar, EARLINET-AERONET (European Aerosol Research Lidar NETwork-AEROSOL rOBOTICS NETwork) and CALIOP data typically show much thinner, more discontinuous cloud structures (Fig. 1, 2). Three separate tabulations of distal ash cloud layer data for the Eyjafjallajökull plume have been published [Jonsson *et al.*, 1996; Ansmann *et al.*, 2011; Winker *et al.*, 2012], and the EARLINET data have been summarized and modelled [Dacre *et al.*, 2015]. The data

Table 1: Examples of main, upper volcanic cloud depth from top to cloud edge. Measured from geostationary imagery in first scene after eruption start (photography for Redoubt). Data from *Bear-Crozier et al.* [2020]; and *Pouget et al.* [2013] and *Holasek et al.* [1996a] (below divider)

<b>Volcano</b>	<b>Eruption start date</b>	<b>Mean height, km ASL</b>	<b>Depth, km</b>	<b>No. layers</b>
Tinakula	Oct 20, 2017, 2350 UT	16.6	4.9	1
Tinakula	Oct 20, 2017, 1930 UT	15.1	3.4	1
Rinjani	Aug 1, 2016, 0345 UT	5.5	4.0	1
Manam	Jul 31, 2015, 0132 UT	13.7	9.2†	2
Sangeang Api	May 11, 2014, 0832 UT	15.4	12.0†	2
<b>Kelud</b>	Feb 13, 2014, 1632 UT	15.3	2.8	1
Manam	Jan 27, 2005, 1400 UT	24.0	3.0	1
Manam	Oct 24, 2004, 2325 UT	18.5	1.5	1
<b>Pinatubo</b>	Jun 15, 1991, 2241 UT	23.6	4.7	1
Redoubt	Apr 21, 1990, 1412 UT	12.0	4.9	2
Mount St. Helens	May 18, 1980, 2020 UT	13.0	1.0	1

† Depth possibly overestimated.

suggest that distal clouds from this tropospheric eruption were typically 0.3-3 km thick, made up of 2-3 layers, with individual layers of 0.3-1.4 km depth, and maximum age of 129 h ( $\approx$  1 week) (Table 2). *Dacre et al.* [2015] estimated a mean and standard deviation of the measured depths of  $1.2 \pm 0.9$  km. The number density of particles in the clouds as they propagated over Europe generally peaked in the micron to submicron range, while the mass density peaked near  $10 \mu\text{m}$  [*Schumann et al.*, 2011], although the larger size modes may be underrepresented [*Ansmann et al.*, 2011].

*Vernier et al.* [2013] using CALIOP data, discerned two or more well-defined layers



in the cloud from Puyehue-Cordon Caulle three weeks after the eruption. Some of the layers showed fold or wrap-around structures (Figure 1a in *Vernier et al.* [2013]), perhaps related to vertical-plane chaotic mixing [*Pierce and Fairlie*, 1993]. Clouds were up to 3 km thick, with individual layers of 0.1-2 km depth, in the upper troposphere-lower stratosphere (UTLS), centered on the tropopause at 8-14 km altitude.

On July 12-13, 1991, 26 days after the last major eruption of Pinatubo, a lidar flight noted numerous stratospheric layers [*Winker and Osborn*, 1992]. The data showed a number of well-defined layers of 0.5-1 km depth between about 14 and 25 km altitude (Figure 1 in *Winker and Osborn* [1992]). Along much of the line of flight there were two layers (22 and 25 km), but in places there were up to five. Within the first day, modeling by *Fero et al.* [2009] is consistent with a mean grain size of 90  $\mu\text{m}$  in the 22-km layer. Although depolarization ratios in the 25-km layer were consistent with mostly sulfur aerosols, even after nearly a month, high backscatter LiDAR depolarization ratios at the base of the 22-km layer were still inexplicably consistent with particles in the 10-100  $\mu\text{m}$  range [*Winker and Osborn*, 1992].

In all studies cited above, distal ash layers were horizontal or tilted relative to the horizon, and had extents in the cross-transport direction of hundreds of km in the troposphere (Eyjafjallajökull), to thousands of km in the stratosphere (Puyehue, Pinatubo).

Once the ash propagated far from vent ( $\geq 11$  hr in the case of a large eruption, e.g., Pinatubo), they no longer retained significant memory of source conditions [*Dacre et al.*, 2015; *Fero et al.*, 2009]. However, simple back trajectories of distal ash clouds for Eyjafjallajökull and Puyehue-Cordon Caullé are generally consistent with theoretically possible cloud heights at the source [*Winker et al.*, 2012; *Vernier et al.*, 2013]. It is not clear that ash was injected at these altitudes at the source, given uncertainties in vertical parcel motion and settling speed, or lack of incorporation thereof in the models [*Madankan et al.*, 2014; *Vernier et al.*, 2013]. This observation suggests that vertical particle motion – settling – is not the sole, or even most, important factor in accounting for vertical positions of ash clouds in the distal region. A more consistent feature is thinning, more sharply defining, and multiplying of the near vent volcanic

cloud features. *Dacre et al.* [2015] suggested that increase and decrease in thickness, are likely due to a balance between vertical wind shear and turbulent diffusion for distal clouds comprised of mostly micron and submicron particles.

## 2.2 Methods

The atmospheric observations summarized in Section 2.1.1 show that both the troposphere and stratosphere are layered in turbulence intensity on a scale of fractions of a kilometer to several kilometers due to both cloud top turbulence and vertical wind shear generation. The ash cloud observations summarized in Section 2.1.2 show that more distal, distinct ash clouds evolve from more proximal, diffuse and thicker clouds. In VATDs, sub-grid dispersal in the vertical direction can be described by a single vertical diffusivity,  $\kappa_z$ , which may take on the same value as the horizontal diffusivity,  $\kappa_h$ ; the result is then uniform or isotropic ash dispersion. Our goal here is to contrast the physical behavior of an ash cloud under conditions of isotropic ( $\kappa_h = \kappa_z = \text{const.}$ ) or constant vertical turbulence ( $\kappa_z \neq \kappa_z(z)$ ), and layered turbulence. We base our methodology on analytical and numerical models using synthetic atmospheres with and without multiple turbulent layers separated by relatively quiescent air.

### 2.2.1 Eulerian Analytical Formulation

In the case of isotropic turbulence, we begin by assuming Cartesian coordinates,  $(x, y, z)$ , with velocity components,  $(u, v, w)$ . The three components of the turbulent diffusivity,  $(\kappa_x, \kappa_y, \kappa_z)$  are the same,  $\kappa$ . The concentration of particles in the  $i$ -size fraction,  $C_i$ , varies in time,  $t$  and space as:

$$\frac{\partial C_i}{\partial t} + \frac{\partial}{\partial x} (uC_i) + \frac{\partial}{\partial y} (vC_i) + \frac{\partial}{\partial z} (wC_i) = \frac{\partial^2}{\partial x^2} (\kappa C_i) + \frac{\partial^2}{\partial y^2} (\kappa C_i) + \frac{\partial^2}{\partial z^2} (\kappa C_i) + \Phi \quad (1)$$

where  $\Phi$  represents the source/sink function, which in the case of ash clouds is mostly represented by aggregation and disaggregation of small particles. In the present case, such processes are set to zero. We assume a two-dimensional system with a point-source in time and space,  $w = w_s$ , the settling speed, and that, following a streamtube, the motion of the volcanic cloud can be characterized by a single downwind coordinate

direction  $s$  – for which the axis is everywhere tangent to the plume centerline, e.g., [Wright, 1977; Hopkins and Bridgman, 1985] – and speed  $U$  in that direction. Under these assumptions, the advection-diffusion equation becomes:

$$\frac{\partial C_i}{\partial t} + \frac{\partial}{\partial s} (UC_i) + \frac{\partial}{\partial z} (w_s C_i) = \frac{\partial^2}{\partial s^2} (\kappa C_i) + \frac{\partial^2}{\partial z^2} (\kappa C_i) \quad (2)$$

with the well-known solution for the impulse initial condition [Csanady, 1980; Roberts and Webster, 2002]:

$$C_i(s, z, t) = \frac{C_{i0}}{4\pi\kappa t} \exp \left[ -\frac{(s - s_0 - Ut)^2 + (z - z_0 - w_s t)^2}{4\kappa t} \right]. \quad (3)$$

It is reasonably clear that the solution is a Gaussian in  $(s, z)$ , in which ash spreads, settles and is blown downwind with time.

The second case is for layered turbulence, in which  $\kappa_z = \kappa_z(z)$ , and generally  $\kappa_z \neq \kappa_h$ . Since a 1D model is instructive in this system, we investigate vertical motions alone. In this system, there is a discontinuity in the diffusive flux at the lower boundary of a turbulent layer because  $\kappa_z$  decreases suddenly, and in this case, the one-dimensional advection-diffusion equation:

$$\frac{\partial}{\partial t} (C_i) + \frac{\partial}{\partial z} (w_s C_i) = \frac{\partial^2}{\partial z^2} (\kappa_z C_i) \quad (4)$$

becomes, in the region of the lower boundary:

$$\frac{\partial}{\partial t} (C_i) + \frac{\partial}{\partial z} (w_s C_i) \approx 0 \quad (5)$$

for  $\kappa_{z,upper} \gg \kappa_{z,lower}$ .

Thus, a step-like concentration gradient develops at the base of the upper layer, as some particles are swept back into it rather than settling across the boundary, hence:

$$C_i(t, z) = H(z)C_i(t) \quad (6)$$

where  $H(z)$  is the Heaviside step function, then:

$$\frac{\partial}{\partial t} (C_i) + \frac{\partial}{\partial z} (w_s C_i) = \frac{\partial C_i}{\partial t} + w_s C_i \frac{\partial H(z)}{\partial z} = 0 \quad (7)$$

Integrating through the layer depth,  $h$ , assuming that turbulence is sufficiently vigorous to homogenize the layer:

$$\frac{\partial C_i}{\partial t} \int_0^h dz = -w_s C_i \int_0^h \delta(z) dz \quad (8)$$

we obtain:

$$\frac{dC_i}{dt} = -\frac{w_s}{h}C_i \quad (9)$$

which has solution:

$$C_i = C_{i0} \exp\left(-\frac{w_s(t-t_0)}{h}\right) \quad (10)$$

In a more quiescent layer below the boundary, particles only settle and are advected downwind, there is little turbulence to enhance persistence within the layer. Thus, for systems in which particle motion is controlled by both turbulent diffusion and settling, turbulent layers can retain particles longer than do quiescent layers because of continuing re-entrainment in eddies. Particles fall relatively rapidly through the quiescent layers because of unhindered settling, sometimes even enhanced by the effects of convective sedimentation [*Hoyal et al.*, 1999a], which is not included in the present model.

## 2.2.2 Lagrangian Formulation

We can gain additional insight by looking at the Lagrangian formulation of the problem. In a Lagrangian framework, common to many ash dispersion models, such as HYSPLIT, movement is given by:

$$\mathbf{r}_{j+1} = \mathbf{r}_j + \mathbf{v} \times \Delta t \quad (11)$$

where  $r$  is the position vector,  $v$  is the velocity vector and  $j$  is a time index, for which  $\Delta t = t_{j+1} - t_j$ . For the vertical,  $z$  component of position:

$$z_{i+1} = z_i + w_s \times \Delta t. \quad (12)$$

If turbulence is added, and assuming no mean vertical flow, this becomes:

$$z_{i+1} = z_i + (w_s + w') \times \Delta t \quad (13)$$

where  $w'$  is the vertical component of an instantaneous turbulence velocity. Note that the direction (up or down) and magnitude of  $w'$  change with time, and therefore effective settling speed,  $w_s + w'$ , can be positive or negative (rising parcel) and of widely

varying magnitude, depending on the ratio of  $w_s$  to  $w'$ . Furthermore,  $w'$  can be related to the turbulent diffusion by:

$$\kappa_z = w' L_o \quad (14)$$

where  $L_o$  is the length scale of the largest eddies, the Ozmidov scale, which must be less than the layer thickness, i.e.,  $L_o < h$ , otherwise layers would be eroded by turbulence.

### 2.2.3 Similarity Theory

Thus, the velocity scales for turbulence and settling are, respectively,  $\bar{w}'$ , the time-mean turbulence velocity, and  $w_s$ . The ratio of these forms the simple dimensionless group,  $\Pi_1$ :

$$\Pi_1 = \frac{w_s}{\bar{w}'}. \quad (15)$$

Likewise, the timescales for the processes can be used to examine the conditions under which diffusion or settling dominates. From Eq 3, the timescale of vertical diffusion,  $\tau_1$ , through a layer of depth,  $h$ , is given as  $\tau_1 = \frac{h^2}{\kappa}$ . From Eq 10, the timescale of settling through the same layer,  $\tau_2$ , is  $\tau_2 = \frac{h}{w_s}$ . The ratio of the two timescales indicates domination of particle transport through the layer by settling or turbulent diffusion in the vertical direction. The ratio is given by the dimensionless group,  $\Pi_2$ :

$$\Pi_2 = \frac{\tau_1}{\tau_2} = \frac{hw_s}{\kappa} \quad (16)$$

Potentially important or critical values of particle size and settling speed,  $w_s$ , turbulence intensity,  $\bar{w}'$ , and eddy diffusivity,  $\kappa_z$  are given in Table 3. In previous work describing the generation of ash cloud layering, values of  $\kappa$  have ranged from  $\kappa_h = 10000 \text{ m}^2/\text{s}$  and  $\kappa_z = 10 \text{ m}^2/\text{s}$  [Fero *et al.*, 2009] using the Puff VATD model, to  $10^{-5} \leq \kappa_z \leq 9$ , with a mean of  $1 \text{ m}^2/\text{s}$ , using the NAME model [Dacre *et al.*, 2015]. Note that in these models, larger-scale eddies are assumed to be characterized by the wind field as described in the NWP model, so that  $\kappa$  represents only the subgrid eddy diffusion. Thus, the effects of diffusion on eddies of the scale of the NWP grid might be poorly resolved. Fero *et al.* [2009] used NWP grids with a resolution of c. 200 km in the horizontal, and 1 km in the vertical, while Dacre *et al.* [2015] used an NWP grid with a resolution of c. 50 km in the horizontal, and 100 m in the vertical. In the



Lagrangian model used in the present contribution, we have explored results for values of effective  $\kappa_z$  ranging from  $3 \times 10^{-6}$  to  $6 \times 10^3$  m<sup>2</sup>/s, while constructing a complete velocity field following the spectral technique discussed in detail in *Jenkins* [1985] and *Bursik* [1998]. To obtain turbulence layering in the spectral model, the Fourier series describing the vertical dispersion is truncated at different wavenumbers in different layers (Table 3).

### 2.3 Numerical Analysis

To illustrate effects of turbulence layering on particle settling and motion, numerical experiments were performed using both Ash3D [*Schwaiger et al.*, 2012] and a Lagrangian model (Section 2.2.2). For a thorough description of the Lagrangian model and the synthetic atmosphere in which it is run, see *Bursik* [1998]. Experimental parameter values of importance used in the models are shown in Table 4. In Section 3, we explore results from Similarity analysis and numerical solutions based on the theoretical development. Numerical solutions are provided for atmospheres both layered and non-layered with respect to turbulence (Table 4).

## 3 Results

In this section, we first investigate expected behavior of ash particles given a layering in atmospheric turbulence structure using Similarity Theory. We then look at numerical results showing what typical particle vertical speed should be, given a synthetic atmospheric turbulence layering (Table 4). Output from several simulations for a synthetic, turbulence-layered atmosphere using different particle size and settling speed are then shown to investigate the potential effects of turbulence layering on particles of different sizes. We then discuss possible turbulence layering in the atmosphere associated with the climactic 1991 Pinatubo eruption, and run simulations in the resulting synthetic atmosphere.

We gain insight into expected behavior using results of the Similarity analysis, and refer to Eqs 15 and 16 to explore asymptotic behavior. In layers for which  $\Pi_1 \parallel \Pi_2 \gg 1$ ,

the turbulent diffusivity is low relative to the settling speed, the timescale of diffusion is therefore long, hence motion is controlled by settling. In layers for which  $\Pi_1 || \Pi_2 \ll 1$ , diffusion is rapid relative to settling, i.e., the timescale of settling is long, hence motion is dominated by diffusion. Note also that as layer thickness,  $h$ , increases, the timescale of diffusion increases faster than does that for settling, meaning it becomes more likely the particles will exit a layer by settling than by diffusion. For a typical diffusivity of  $\kappa = 1 \text{ m}^2/\text{s}$  in the UTLS [Wilson, 2004] at 10 km altitude, and layer of depth  $h = 1 \text{ km}$ , the critical settling speed,  $w_{s,crit}$ , dividing settling from diffusion dominated motion is c. 1 m/s, which would correspond to a pumice particle of diameter c. 100  $\mu\text{m}$  at about 2400 kg/cu m (e.g., [Scollo *et al.*, 2005]).

Numerical results for a layered system (Fig. 3) are shown in Figure 4. Figure 3 is based on the observations of Cho *et al.* [2003], who point out two layers of especially striking turbulence from 2-2.7 km and 3.8-4.2 km (Fig. 3), but do not give specific values for turbulence intensity. We therefore apply high turbulence in these two layers through a simple Lagrangian random walk, and in other layers, low turbulence. The largest particles, in this case  $> 1 \text{ mm}$ , are dominated by settling and show little sensitivity to turbulence (Fig. 4a). Intermediate sized particles,  $\sim 10 - 250 \mu\text{m}$  (Fig. 4b, c) in the more turbulent layers initiate a random walk, being “stuck” within the eddies of the turbulent layer. These particles are subjected to turbulence-hindered settling in the more turbulent layers. In these cases, consider the lower boundary of a layer with strong turbulence. All the particles there are subject to a random walk. They have a 50% percent probability of going up, and a 50% probability of going down. Those particles sent above the lower boundary due to turbulence are sent to a position higher above the boundary than their original position at the boundary. This will give them a greater chance to spend a longer time in the turbulent layer, whether or not one considers settling. Thus, for those layers dominated by the random walk and dispersion,  $\Pi_1 \leq 1$ , Eq 10 holds, and the behavior seen in Figures 4b, c occurs. The motion of the smallest particles, here c. 1  $\mu\text{m}$  (Fig. 4d), is dominated by turbulent diffusion. The particles spread slowly both upward and downward in the less turbulent layers, and rapidly in the more turbulent layers, causing them to have relatively low mean

concentration.

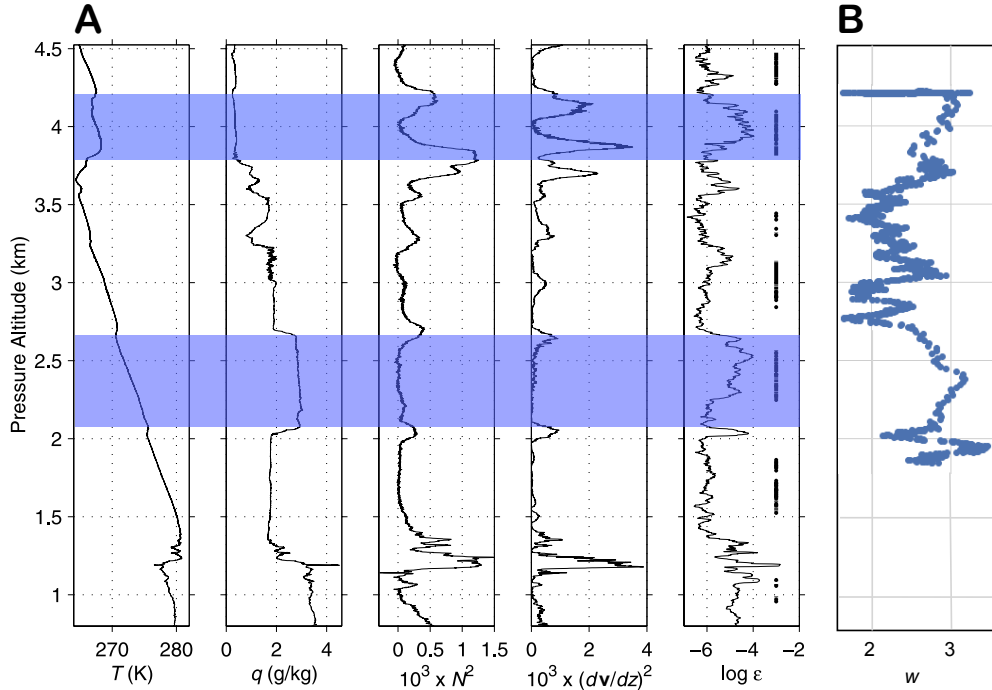


Figure 3: Turbulent tropospheric layers (shaded) indicated by constant mixing ratio ( $q$ ), high turbulent energy dissipation rate ( $\log \varepsilon$ ), and bounded by high shear ( $(dU/dz)^2$ ). Modified from *Cho et al.* [2003]. Shaded layers are used in simplified layer models (Table 4).

In contrast, and following from Eq 3, spread from a point source in a VATD model, with isotropic turbulence and a wind of constant speed with height, is shown in Figure 7. Ash diffuses and progressively spreads from the source as the center of mass descends at the settling speed. Using a higher settling speed, the rate at which the center of mass descends increases, but the rate at which the particles disperse from the center of mass remains constant. Thus, at any one height below the source, particles with a higher settling speed should be spread less distance from the source.

### 3.1 Application to 1991 Pinatubo eruption

There are no direct observations of turbulence values associated with the climactic 1991 eruption of Pinatubo. As noted in Section 2.2.3, *Fero et al.* [2009] explored values of  $\kappa_z = 10$  and  $\kappa_h = 10^4$  m<sup>2</sup>/s for the eruption. Given understanding of turbulence

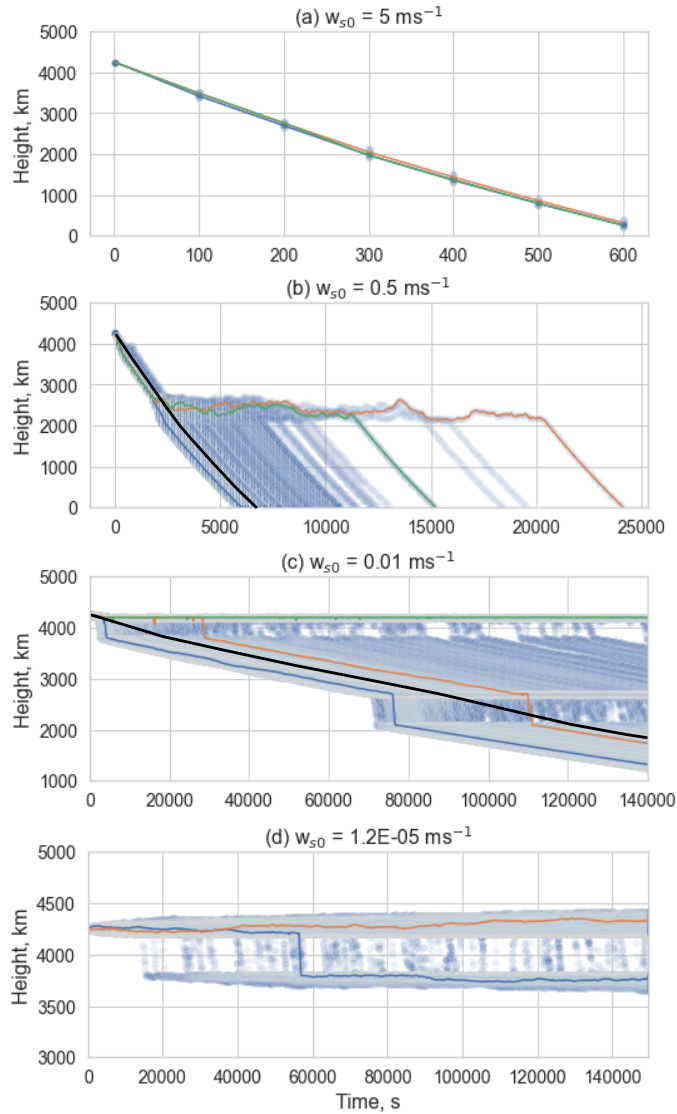


Figure 4: Longitudinal time-section through Lagrangian dispersion model showing paths of volcanic particles settling through turbulent layers, in which suspension is enhanced. This is output based on layers in Fig. 3. See Table 4.

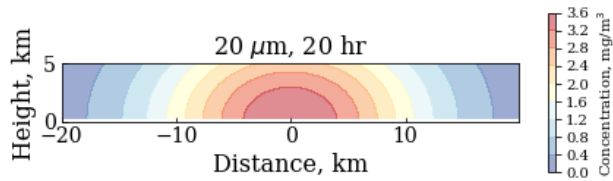


Figure 5: Crosswind section through Ash3D output (Table 4), with instantaneous source and no wind shear, showing advection, settling and isotropic dispersal of  $10\mu\text{m}$  ash.

generation, we can nevertheless speculate with some assurance that cloud top turbulence generation was probably strong above the Pinatubo umbrella cloud [Vasseur and Vanhoenacker, 1998], and that wind shear generated turbulence near the tropopause at 16-17 km was probably strong due to the shift from southwesterly to northeasterly winds at that altitude [Fero et al., 2009]. This assessment is consistent with the general observation that the most intense level of clear-air turbulence development in the lower atmosphere is the tropopause [Clayson and Kantha, 2008]. We therefore construct a speculative turbulence layering for the eruption based on these considerations.

The main umbrella cloud of the climactic 1991 Pinatubo eruption was centered between 24 to 26 km height and  $\sim 3 - 6$  km thick, although ash was injected as low as 17 km and as high as 40 km [Holasek et al., 1996a; Fero et al., 2009]. From this initial umbrella cloud, the development and separation of layers rapidly evolved into two main clouds, the first rich in larger particles and centered at the tropopause ( $\sim 16 - 17$  km); the second, a higher cloud rich in  $\text{SO}_2$  and particle that remained centered near the neutral buoyancy height of 25 km [Fero et al., 2009]. These two main ash transport regions persisted, centered around 14-16 and 22-25 km [Winker and Osborn, 1992] until at least about a month after the eruption. Based on possible/likely generation of stronger turbulence by cloud-top convective and wind shear mechanisms, respectively, these two regions are given higher values of turbulence intensity in layered, Lagrangian model runs (Table 4).

With the atmosphere having these speculative intensely turbulent layers, we modeled the settling of 1 to 4000  $\mu\text{m}$  particles from the Pinatubo cloud for periods up to a week. Although particles as large as 1000  $\mu\text{m}$  were affected by the turbulence layering (Fig. 6), we focus on the results for 10 and 30  $\mu\text{m}$  particles at 18hr, as these were dominant in parts of the cloud for periods up to nearly a month (Section 2.1.2) [Winker and Osborn, 1992], and as the 18-hr time window is particularly important to VAAC ash cloud forecasting. 18 hr is the length of the forecast window typically issued in volcanic ash advisories (VAA) and shown in volcanic ash graphics (VAG) issued by the VAACs. The results for these particle sizes are consistent with observations of cloud heights, particle sizes (Section 2.1.2) and speculative layering within them (Fig.



7). Given particles released from heights ranging from 23 to 27 km, after 18hr, 10  $\mu\text{m}$  particles are concentrated in the 24-25 km high-turbulence layers, whereas 30  $\mu\text{m}$  particles are mostly spread throughout the 14.5 to 19 km high-turbulence layer. While both boundaries of the 24-25 km layer are sharp, 30  $\mu\text{m}$  particles, predominantly in the lower layer, are concentrated at and above the 14.5 km lower boundary and around the 19 km upper boundary (Fig. 8). This concentration near the boundaries results from the recirculation of particles from the strongly turbulent layer into the overlying less turbulent layer near the 19 km boundary (e.g., Fig. 4d), and settling modified behavior near the lower boundary (e.g., Fig. 4b). The persistence of the particles in the turbulent layers, and more specifically their concentration near the lower boundary of the lower layer by turbulence, may explain the layering and inexplicable concentration near the base of particle-rich layers observed by *Winker and Osborn* [1992].

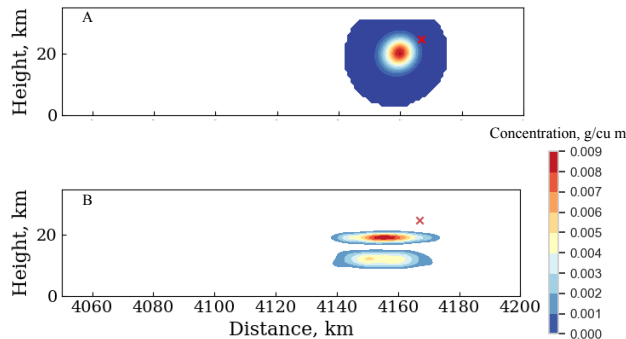


Figure 6: **(a)** Downwind section through Ash3D output (Table 4), with instantaneous source and no wind shear, showing advection, settling and isotropic dispersal of 1000  $\mu\text{m}$  particles, 50 min after eruption. **(b)** Downwind section through Lagrangian output (Table 4), with instantaneous source and no wind shear, showing dispersal of ash in layered turbulence.

## 4 Discussion and Conclusions

In the present work, we have presented data and models on near-vent and distal volcanic cloud morphology and ash loading. We have performed numerical experiments comparing dispersal in an atmosphere with constant  $\kappa$  and variable  $\kappa_z$  with height. The observational data suggest that distal clouds of depth  $\mathcal{O}[0.1 \text{ to } 1]$  km develop from

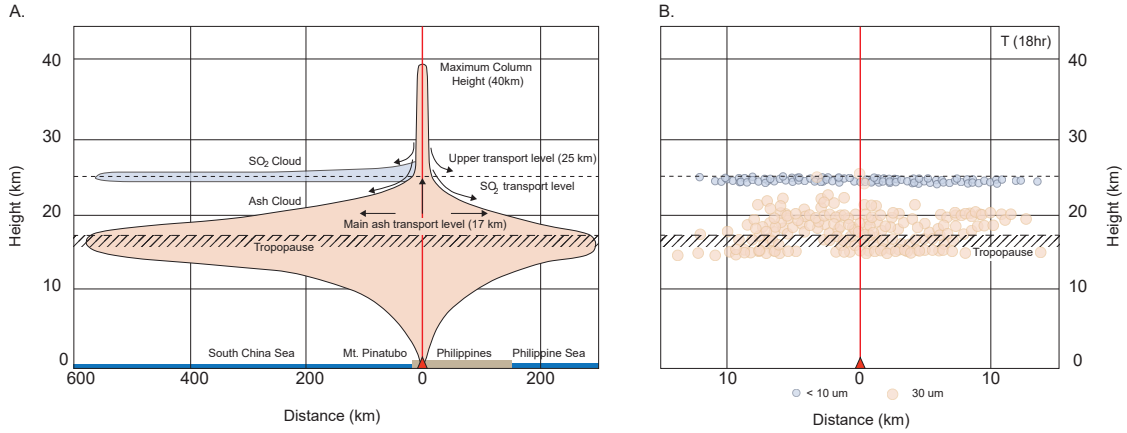


Figure 7: **(a)** Schematic longitudinal section through Pinatubo ash cloud at 5hr, based on *Fero et al.* [2009]. Box on left shows range of volcanic cloud heights after 26 days according to *Winker and Osborn* [1992]. **(b)** Cross section through Lagrangian dispersion model for 10 and 30  $\mu\text{m}$  particles (Table 4 with turbulence layered atmosphere, showing advection, settling and non-isotropic ash dispersal. Red  $\times$  is point of origin for particles, and color gradient is scaled to concentration in both.

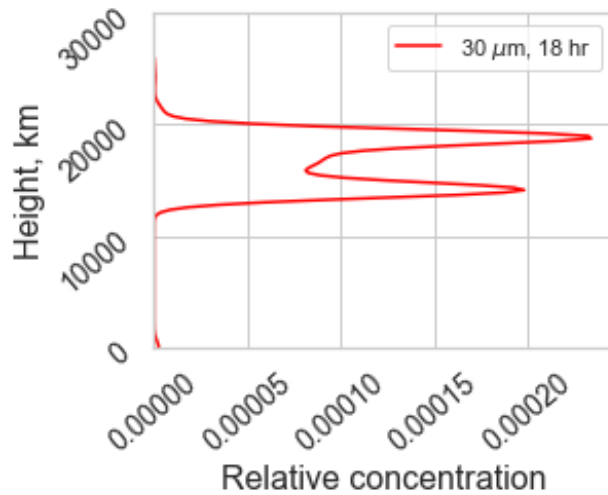


Figure 8: Relative concentration profile of the 30 $\mu\text{m}$  particles after 18 hr showing peaks in concentration near top and bottom of 14.5-19 km turbulent layer.

near-vent clouds of  $\mathcal{O}[1-10]$  km depth. The downwind clouds occur at heights consistent with the original eruption column heights for both tropospheric and stratospheric eruptions. The depth range of the distal layers, being generally less than the near-vent depth range, and the common stacking of distal layers, suggest that their development

is controlled by atmospheric processes. The observations are consistent with the working hypothesis that the layering of the atmosphere in turbulence intensity, generally causing alternating suspension and settling dominated behavior of appropriately sized particles, in the present experiments, those of  $\mathcal{O}[10-100] \mu\text{m}$ , is a cause of distal layer morphology. Particles larger than those in this size range are dominated by settling and show little sensitivity to variations in turbulence intensity, while the motion of smaller, micron sized particles, is dominated by diffusion, with such particles being preferentially swept out of more turbulent layers. The numerical results are consistent with and explain in more detail those of *Dacre et al.* [2015] that the motion and layering of  $\mathcal{O}[1-10] \mu\text{m}$  particle clouds is driven by a balance between wind shear and turbulent diffusion.

In addition to the near-vent volcanic processes modifying ash cloud layering, atmospheric processes produce distal layered ash clouds, which are often multilayered due to multiple, alternating layers of turbulent and quiescent air. The distal ash layers scale to the depth of the alternating turbulent and quiescent layers in the atmosphere, which are  $\mathcal{O}[0.1 - 1]$  km deep. The model outputs (Fig. 7) are not inconsistent with those of VATD and backtrajectory models, in which homogeneous turbulence can be associated with layers, given pre-existing ash cloud layering at the source vent, or wind shear [*Devenish et al.*, 2012; *Folch et al.*, 2012; *Heinold et al.*, 2012; *Winker et al.*, 2012; *Vernier et al.*, 2013]. It is likely that shear together with layering in turbulent diffusivity controls thickness of distal layers for periods of days to perhaps a month by hindering settling of particles in the 1-1000  $\mu\text{m}$  range [*Dacre et al.*, 2015]; note that the wind shear and turbulence layering processes are not mutually exclusive [*Cho et al.*, 2003].

The results suggest that to better forecast the position and morphology of ash clouds for aviation safety and other purposes in VATDs, the vertical characteristics of the atmosphere need to be better resolved and characterized, particularly in the 18-hour time window critical to forecasting in VAAs and VAGs. Because of the importance of turbulence and moisture to layer formation, it is critical that these two parameters especially be estimated well, and at as high a vertical resolution as possible. Specifically,

if appropriate sonde or other high vertical resolution data are available, they should be used to calculate heights of potentially elevated  $\kappa$ , to be used as deterministic input into VATDs for the source ash-height injection time history. Thus, it is possible that the source ash-height injection time history could be determined *a priori*, rather than found *a posteriori* through inversion [Stohl *et al.*, 2011; Kristiansen *et al.*, 2015]. Being able to provide such information *a priori* could have a strong positive impact on forecasting the future heights and thicknesses of ash clouds for aviation using VATDs.

**Acknowledgments** . Simon Carn is thanked for initial interest and encouragement in this work. Bruce Pitman is thanked for useful conversation on this topic. Larry Mastin gave valuable feedback on an earlier version of the ms regarding related work. Q. Yang was funded by the Earth Observatory of Singapore. We thank the creators of Ash3D, Pandas, Matplotlib and Seaborn for excellent software tools enabling this research.

The following abbreviations are used in this manuscript:

AERONET	AERosol RObotic NETwork
BT	Brightness Temperature
CALIOP	Cloud-Aerosol Lidar with Orthogonal Polarization
EARLINET	European Aerosol Research Lidar Network
IAVW	International Airways Volcano Watch
RH	Relative Humidity
UTLS	Upper Troposphere - Lower Stratosphere
VATD	Volcanic Ash Transport and Dispersal

## References

Ansmann, A., et al., Ash and fine-mode particle mass profiles from earlinet-aeronet observations over central europe after the eruptions of the eyjafjallajökull volcano in 2010, *Journal of Geophysical Research: Atmospheres*, 116(D20), doi:10.1029/2010JD015567, 2011.

- Barat, J., Some characteristics of clear-air turbulence in the middle stratosphere, *Journal of the Atmospheric Sciences*, 39(11), 2553–2564, 1982.
- Barr, S., Skirt clouds associated with the soufriere eruption of 17 april 1979, *Science*, 216(4550), 1111–1112, 1982.
- Bear-Crozier, A., S. Pouget, M. Bursik, E. Jansons, J. Denman, A. Tupper, and R. Rustowicz, Automated detection and measurement of volcanic cloud growth: towards a robust estimate of mass flux, mass loading and eruption duration, *Natural Hazards*, pp. 1–38, 2020.
- Britter, R. E., and J. E. Simpson, A note on the structure of the head of an intrusive gravity current, *Journal of Fluid Mechanics*, 112, 459–466, doi:10.1017/S0022112081000517, 1981.
- Bursik, M., Tephra dispersal, in *The Physics of Explosive Volcanic Eruptions, Special Publications*, vol. 145, edited by J. S. Gilbert and R. S. J. Sparks, pp. 117–146, Geological Society of London, illus. incl. sketch maps, 1998.
- Carazzo, G., and A. M. Jellinek, A new view of the dynamics, stability and longevity of volcanic clouds, *Earth and Planetary Science Letters*, 325, 39–51, 2012.
- Carazzo, G., and A. M. Jellinek, Particle sedimentation and diffusive convection in volcanic ash-clouds, *Journal of Geophysical Research*, 118, 1420–1437, 2013.
- Casadevall, T. J., Volcanic ash and aviation safety: Proceedings of the first international symposium on volcanic ash and aviation safety, *U.S. Geological Survey Bulletin*, 2047, 450, 1994.
- Chakraborty, P., G. Gioia, and S. Kieffer, Volcán reventador’s unusual umbrella, *Geophysical research letters*, 33(5), 2006.
- Cho, J. Y., R. E. Newell, B. E. Anderson, J. D. Barrick, and K. L. Thornhill, Characterizations of tropospheric turbulence and stability layers from aircraft observations, *Journal of Geophysical Research: Atmospheres*, 108(D20), 2003.



- Clayson, C. A., and L. Kantha, On turbulence and mixing in the free atmosphere inferred from high-resolution soundings, *Journal of Atmospheric and Oceanic Technology*, 25(6), 833–852, 2008.
- Csanady, D. T., Turbulent diffusion in the environment, *D.Reidel Publishing Co*, p. 248p, dordrecht, 1980.
- Dacre, H., A. Grant, N. Harvey, D. Thomson, H. Webster, and F. Marengo, Volcanic ash layer depth: Processes and mechanisms, *Geophysical Research Letters*, 42(2), 637–645, 2015.
- Dehghan, A., W. K. Hocking, and R. Srinivasan, Comparisons between multiple in-situ aircraft turbulence measurements and radar in the troposphere, *Journal of Atmospheric and Solar-Terrestrial Physics*, 118, 64–77, 2014.
- Devenish, B., D. Thomson, F. Marengo, S. Leadbetter, H. Ricketts, and H. Dacre, A study of the arrival over the united kingdom in april 2010 of the eyjafjallajökull ash cloud using ground-based lidar and numerical simulations, *Atmospheric Environment*, 48, 152 – 164, doi:<https://doi.org/10.1016/j.atmosenv.2011.06.033>, volcanic ash over Europe during the eruption of Eyjafjallajökull on Iceland, April-May 2010, 2012.
- Fero, J., S. N. Carey, and J. T. Merrill, Simulating the dispersal of tephra from the 1991 pinatubo eruption: implications for the formation of widespread ash layers, *Journal of Volcanology and Geothermal Research*, 186(1-2), 120–131, 2009.
- Folch, A., A. Costa, and S. Basart, Validation of the fall3d ash dispersion model using observations of the 2010 eyjafjallajökull volcanic ash clouds, *Atmospheric Environment*, 48, 165 – 183, doi:<https://doi.org/10.1016/j.atmosenv.2011.06.072>, volcanic ash over Europe during the eruption of Eyjafjallajökull on Iceland, April-May 2010, 2012.
- Gage, K., J. Green, and T. VanZandt, Use of doppler radar for the measurement

- of atmospheric turbulence parameters from the intensity of clear-air echoes, *Radio Science*, 15(2), 407–416, 1980.
- Harvey, N. J., N. Huntley, H. F. Dacre, M. Goldstein, D. Thomson, and H. Webster, Multi-level emulation of a volcanic ash transport and dispersion model to quantify sensitivity to uncertain parameters., *Natural hazards and earth system sciences.*, 18(1), 41–63, 2018.
- Heinold, B., I. Tegen, R. Wolke, A. Ansmann, I. Mattis, A. Minikin, U. Schumann, and B. Weinzierl, Simulations of the 2010 eyjafjallajökull volcanic ash dispersal over europe using cosmo–muscat, *Atmospheric Environment*, 48, 195 – 204, doi: <https://doi.org/10.1016/j.atmosenv.2011.05.021>, volcanic ash over Europe during the eruption of Eyjafjallajökull on Iceland, April-May 2010, 2012.
- Holasek, R. E., S. Self, and A. W. Woods, Satellite observations and interpretation of the 1991 mount pinatubo eruption plumes, *Journal of Geophysical Research*, 12(27), 635–27, 1996a.
- Holasek, R. E., A. W. Woods, and S. Self, Experiments on gas-ash separation processes in volcanic umbrella clouds, *Journal of Volcanology Geothermal Research*, 70, 169–181, 1996b.
- Hopkins, A. T., and C. J. Bridgman, A volcanic ash transport model and analysis of mount st. helens ashfall, *Journal of Geophysical Research*, 90, 10,620–10,630, 1985.
- Hoyal, D. C. J. D., M. I. Bursik, and J. F. Atkinson, Setting-driven convection; a mechanism of sedimentation from stratified fluids, *Journal of Geophysical Research, C, Oceans*, 104(4), 7953–7966, illus. incl. 1 table, 1999a.
- Hoyal, D. C. J. D., M. I. Bursik, and J. F. Atkinson, The influence of diffusive convection on sedimentation from buoyant plumes, *Marine Geology*, 159(1-4), 205–220, 1999b.
- Jenkins, A., Simulation of turbulent dispersion using a simple random model of the

- flow field, *Applied Mathematical Modelling*, 9, 239–245, doi:0307-904X/85/04239-07, 1985.
- Jonsson, H. H., J. C. Wilson, C. A. Brock, J. E. Dye, G. V. Ferry, and K. R. Chan, Evolution of the stratospheric aerosol in the northern hemisphere following the june 1991 volcanic eruption of mount pinatubo: Role of tropospheric-stratospheric exchange and transport, *Journal of Geophysical Research*, 101, 1553–1570, 1996.
- Kristiansen, N. I., A. Prata, A. Stohl, and S. A. Carn, Stratospheric volcanic ash emissions from the 13 february 2014 kelut eruption, *Geophysical Research Letters*, 42(2), 588–596, 2015.
- Madankan, R., et al., Computation of probabilistic hazard maps and source parameter estimation for volcanic ash transport and dispersion, *Journal of Computational Physics*, 271(0), 39 – 59, doi:http://dx.doi.org/10.1016/j.jcp.2013.11.032, *frontiers in Computational Physics Modeling the Earth System*, 2014.
- Maekawa, Y., S. Fukao, M. Yamamoto, M. D. Yamanaka, T. Tsuda, S. Kato, and R. F. Woodman, First observation of the upper stratospheric vertical wind velocities using the jicamarca vhf radar, *Geophysical research letters*, 20(20), 2235–2238, 1993.
- Marenco, F., B. Johnson, K. Turnbull, S. Newman, J. Haywood, H. Webster, and H. Ricketts, Airborne lidar observations of the 2010 eyjafjallajökull volcanic ash plume, *Journal of Geophysical Research: Atmospheres*, 116(D20), 2011.
- Mazzocchi, M., F. Hansstein, and M. Ragona, The 2010 volcanic ash cloud and its financial impact on the european airline industry, in *CESifo Forum*, vol. 11, pp. 92–100, München: ifo Institut für Wirtschaftsforschung an der Universität München, 2010.
- Nastrom, G., and F. Eaton, The coupling of gravity waves and turbulence at white sands, new mexico, from vhf radar observations, *Journal of Applied Meteorology*, 32(1), 81–87, 1993.

- Pavelin, E., J. A. Whiteway, R. Busen, and J. Hacker, Airborne observations of turbulence, mixing, and gravity waves in the tropopause region, *Journal of Geophysical Research: Atmospheres*, 107(D10), ACL-8, 2002.
- Pavolonis, M. J., A. K. Heidinger, and J. Sieglaff, Automated retrievals of volcanic ash and dust cloud properties from upwelling infrared measurements, *Journal of Geophysical Research: Atmospheres*, 118(3), 1436–1458, 2013.
- Pierce, R. B., and T. D. A. Fairlie, Chaotic advection in the stratosphere: Implications for the dispersal of chemically perturbed air from the polar vortex, *Journal of Geophysical Research: Atmospheres*, 98(D10), 18,589–18,595, 1993.
- Pouget, S., M. Bursik, P. Webley, J. Dehn, and M. Pavolonis, Estimation of eruption source parameters from umbrella cloud or downwind plume growth rate, *Journal of Volcanology and Geothermal Research*, 258, 100–112, 2013.
- Pouget, S., M. Bursik, C. G. Johnson, A. J. Hogg, J. C. Phillips, and R. S. J. Sparks, Interpretation of umbrella cloud growth and morphology: implications for flow regimes of short-lived and long-lived eruptions, *Bulletin of Volcanology*, 78(1), 1–19, doi: 10.1007/s00445-015-0993-0, 2016.
- Prata, F., M. Woodhouse, H. E. Huppert, A. Prata, T. Thordarson, and S. Carn, Atmospheric processes affecting the separation of volcanic ash and so<sub>2</sub> in volcanic eruptions: inferences from the may 2011 grímsvötn eruption, *Atmospheric Chemistry and Physics*, 17(17), 10,709–10,732, 2017.
- Roberts, P. J., and D. R. Webster, Turbulent diffusion, in *Environmental Fluid Mechanics: Theories and Applications*, edited by H. H. Shen, A. H. Cheng, K.-H. Wang, M. H. Teng, and C. C. Liu, pp. 7–45, ASCE Press, Reston, Virginia, 2002.
- Sato, K., H. Hashiguchi, and S. Fukao, Gravity waves and turbulence associated with cumulus convection observed with the uhf/vhf clear-air doppler radars, *Journal of Geophysical Research: Atmospheres*, 100(D4), 7111–7119, 1995.

- Schumann, U., et al., Airborne observations of the eyjafjalla volcano ash cloud over europe during air space closure in april and may 2010, *Atmos. Chem. Phys.*, *11*, 2245–2279, doi:10.5194/acp-11-2245-2011, 2011.
- Schwaiger, H. F., R. P. Denlinger, and L. G. Mastin, Ash3d: A finite-volume, conservative numerical model for ash transport and tephra deposition, *Journal of Geophysical Research: Solid Earth*, *117*(B4), 2012.
- Scollo, S., M. Coltelli, F. Prodi, M. Folegani, and S. Natali, Terminal settling velocity measurements of volcanic ash during the 2002–2003 etna eruption by an x-band microwave rain gauge disdrometer, *Geophysical Research Letters*, *32*(10), 2005.
- Sharman, R. D., S. B. Trier, T. P. Lane, and J. D. Doyle, Sources and dynamics of turbulence in the upper troposphere and lower stratosphere: A review,, *Geophys Res Lett*, *39*, doi:10.1029/2012GL051996, 2012.
- Sparks, R. S. J., M. I. Bursik, S. N. Carey, J. S. Gilbert, L. S. Glaze, H. Sigurdsson, and A. W. Woods, *Volcanic Plumes*, John Wiley & Sons, London, 574p., 1997.
- Stohl, A., et al., Determination of time-and height-resolved volcanic ash emissions and their use for quantitative ash dispersion modeling: the 2010 eyjafjalla-jökull eruption, *Atmospheric Chemistry and Physics*, *11*, 4333–4351, 2011.
- Thorsteinsson, T., T. Jóhannsson, A. Stohl, and N. I. Kristiansen, High levels of particulate matter in iceland due to direct ash emissions by the eyjafjalla-jökull eruption and resuspension of deposited ash, *Journal of Geophysical Research: Solid Earth*, *117*(B9), 2012.
- Thouret, V., J. Y. Cho, R. E. Newell, A. Marenco, and H. G. Smit, General characteristics of tropospheric trace constituent layers observed in the mozaic program, *Journal of Geophysical Research: Atmospheres*, *105*(D13), 17,379–17,392, 2000.
- Tupper, A., S. Carn, J. Davey, Y. Kamada, R. Potts, F. Prata, and M. Tokuno, An evaluation of volcanic cloud detection techniques during recent significant eruptions in the western 'ring of fire', *Remote Sensing of Environment*, *91*(1), 27–46, 2004.

- Tupper, A., I. Itikarai, M. Richards, F. Prata, S. Carn, and D. Rosenfeld, Facing the challenges of the international airways volcano watch: the 2004/05 eruptions of manam, papua new guinea, *Weather and Forecasting*, *22*(1), 175–191, 2007.
- Tupper, A., C. Textor, M. Herzog, and H.-F. Graf, Tall clouds from small eruptions: modelling the sensitivity of eruption height and fine ash fallout to tropospheric instability, *Natural Hazards*, doi:10.1007/s11069-009-9433-9, 2009.
- Vasseur, H., and D. Vanhoenacker, Characteristics of tropospheric turbulent layers from radiosonde data, *Electronic Letters*, *34*, 318–319, 1998.
- Vernier, J.-P., et al., An advanced system to monitor the 3d structure of diffuse volcanic ash clouds, *Journal of applied meteorology and climatology*, *52*(9), 2125–2138, 2013.
- Wilson, R., Turbulent diffusivity in the free atmosphere inferred from mst radar measurements: a review, *Annales Geophysicae*, *22*, 3869–3887, 2004.
- Wilson, R., H. Luce, H. Hashiguchi, N. Nishi, and Y. Yabuki, Energetics of persistent turbulent layers underneath mid-level clouds estimated from concurrent radar and radiosonde data, *Journal of Atmospheric and Solar-Terrestrial Physics*, *118*, 78–89, 2014.
- Winker, D., and M. Osborn, Preliminary analysis of observations of the pinatubo volcanic plume with a polarization-sensitive lidar, *Geophysical research letters*, *19*(2), 171–174, 1992.
- Winker, D., Z. Liu, A. Omar, J. Tackett, and D. Fairlie, Caliop observations of the transport of ash from the eyjafjallajökull volcano in april 2010, *Journal of Geophysical Research: Atmospheres*, *117*(D20), 2012.
- Woods, A. W., and J. Kienle, The dynamics and thermodynamics of volcanic clouds: Theory and observations from the april 15 and april 21, 1990 eruptions of redoubt volcano, alaska, *Journal of Volcanology and Geothermal Research*, *62*(1-4), 273–299, 1994.

Wright, S. J., Effects of ambient crossflows and density stratification on the characteristic behavior of round turbulent buoyant jets, *W.M. Keck Laboratory, Caltech, Pasadena, Report KH-R-36*, 1977.

Zidikheri, M. J., C. Lucas, and R. J. Potts, Estimation of optimal dispersion model source parameters using satellite detections of volcanic ash, *Journal of Geophysical Research: Atmospheres*, *122*, 8207–8232, doi:<https://doi.org/10.1002/2017JD026676>, 2017.

Zidikheri, M. J., C. Lucas, and R. J. Potts, Quantitative verification and calibration of volcanic ash ensemble forecasts using satellite data, *Journal of Geophysical Research: Atmospheres*, *123*, 4135–4156, doi:<https://doi.org/10.1002/2017JD027740>, 2018.

Table 2: Measured distal Eyjafjallajökull cloud depths from CALIOP lidar. Data from *Winker et al.* [2012] (top section), *Marenco et al.* [2011] (middle) and *Schumann et al.* [2011] (bottom).

Note that number of layers varies with spatial position.

Date	Cloud	Height range, km ASL	Depth, km	Age, hr	No. layers
Apr 15	20100415	1.41–3.23	0.51	< 6	–
Apr 16	20100416-a	3.77–5.50	0.58	30	> 1
Apr 16	20100416-b	1.97–7.27	0.67	24	> 1
Apr 17	20100417-a	0.20–6.28	0.76	42	1
Apr 17	20100417-b	0.05–4.00	0.61	42	1
Apr 18	20100418-a	3.14–5.59	0.81	66	–
Apr 18	20100418-b	3.75–6.49	0.86	66	–
Apr 19	20100419-a	3.20–5.26	1.06	71	–
Apr 19	20100419-c	2.48–3.94	0.45	30	–
Apr 19	20100419-d	4.63–5.20	0.41	114–126	–
Apr 20	20100420	0.05–1.88	1.08	20–24	–
May 4	20100504	2.3–5.5	0.5	–	1-2
May 5	20100505	2.4–4.5	0.9	–	1-2
May 14	20100514	5.1–8.1	1.1	–	1-3
May 16	20100516	3.4–5.5	1.2	–	1-3
May 17	20100517	3.5–5.6	1.3	–	1-3
May 18	20100518	2.5–4.9	0.9	–	1-3
<b>Apr 19</b>	20100419-1	3.9-5.6	1.7	105-111	> 1
Apr 19	20100419-2	3.5-3.8	0.3	104-108	1
Apr 19	20100419-3	3.9-4.2	0.3	105-108	1
Apr 22	20100422-4	0.7-5.5	–	49-50	diffuse
Apr 23	20100423-5	2.1-3.4	1.3	40-58	> 1
May 2	20100502-6	1.6-3.7	2.1	7.1-12	> 1
May 9	20100509-7	3.5-4.9	1.4	97-129	1
May 13	20100513-8	2.8-5.4	0.4-0.7	71-78	1 tilted
May 16	20100516-9	3.6-7.0	3.4	58-66	> 1
May 17	20100517-10	2.5-3.9	1.4	66-67	> 1



Table 3: Values of dimensionless groups for different particle sizes and layer thicknesses.

Diameter $\mu\text{m}$	Settling speed, m/s	$\Pi_1$		$\Pi_2$	
	$w_s$ , m/s	$\bar{w}' \sim 0.31$ m/s	$\bar{w}' \sim 4.9$ m/s	$\kappa_z = 0.098$ m <sup>2</sup> /s	$\kappa_z = 5800$ m <sup>2</sup> /s
4000	5.0e+00	1.6e+01	1.0e+00	51020.4	8.6e-01
1000	3.0e+00	9.7e+00	6.1e-01	30612.2	5.2e-01
250	5.0e-01	1.6e+00	1.0e-01	5102.0	8.6e-02
100	1.0e-01	3.2e-01	2.0e-02	1020.4	1.7e-02
30	1.0e-02	3.2e-02	2.0e-03	102.0	1.7e-03
10	8.0e-04	2.6e-03	1.6e-04	8.2	1.4e-04
1	1.2e-05	3.9e-05	2.4e-06	0.1	2.1e-06

Table 4: Simulation parameters. Duration refers to emission from vent.

Parameter↓—Model→	Test, nonlayered	Test, layered	Pinatubo
Simulation type	VATD	Lagrangian	Lagrangian and VATD
Source type	Point	Point	Point
Source height, km	4.2	4.2 - 10	24-27
Particle size, $\mu\text{m}$	10-100	1-4000	1-1000
Settling speeds tested, m/s	8.0e-04 – 1.0e-01	1.2e-05–1.1	1.2e-05–1.1
Amount	0.01 km <sup>3</sup>	1000 parcels	1000 parcels
Duration of release	0.2 hr	Instantaneous	Instantaneous
Turbulent layer heights, km	–	2.1-2.7, 3.8-4.2	24-25, 14.5-19
Turbulent diffusivity, m <sup>2</sup> /s		0.098-5800 <sup>1</sup>	0.098-5800

<sup>1</sup>Values are for layers with weaker and stronger turbulence, respectively. Intermediate values also explored.